Observational Study

Medicine

OPEN

Reverse predictive analysis of Rhizoma Pinelliae and Rhizoma Coptidis on differential miRNA target genes in lung adenocarcinoma

Tianwei Meng, MM[a], Jiawen Liu, MM[a], Hong Chang, MD[b,*], Rui Qie, MD[c]

Abstract

To use bioinformatics and network analysis to reveal the mechanism of "Rhizoma Pinelliae-Rhizoma Coptidis" herb pair in the treatment of lung adenocarcinoma. The target and pathway of "Rhizoma Pinelliae-Rhizoma Coptidis" herb pair in the treatment of lung adenocarcinoma were explored by online databases and network analysis tools, and the potential biomarkers of "Rhizoma Pinelliae-Rhizoma Coptidis" herb pair in the treatment of lung adenocarcinoma were predicted in reverse. A total of 59 traditional Chinese medicine compounds and 510 drug targets were screened in this study. A total of 25 micro-RNAs and 15,323 disease targets were obtained through GEO2R software analysis. In the end, 294 therapeutic targets and 47 core targets were obtained. A total of 186 gene ontology enrichment assays were obtained, and core therapeutic targets play multiple roles in biological processes, molecular functions, and cellular composition. Kyoto encyclopedia of genes and genomes pathway enrichment analysis showed that the core targets were mainly enriched in cancer-related pathways, immune-related pathways, endocrine-related pathways, etc, among which the non-small cell lung cancer pathway was the most significant core pathway. Molecular docking shows that the compound and the target have good binding ability. "Rhizoma Pinelliae-Rhizoma Coptidis" herb pair plays a mechanism of action in the treatment of lung adenocarcinoma through multiple targets and pathways. miR-5703, miR-3125, miR-652-5P, and miR-513c-5p may be new biomarkers for the treatment of lung adenocarcinoma.

Abbreviations: EGFR = epidermal growth factor receptor, FoxO = forkhead box O, GO = gene ontology, KEGG = Kyoto encyclopedia of genes and genomes, LUAD = lung adenocarcinoma, miRNA = micro RNA, PPI = protein-protein interaction.

Keywords: bioinformatics, lung adenocarcinoma, miRNA, molecular docking, Rhizoma Coptidis, Rhizoma Pinelliae

1. Introduction

Lung adenocarcinoma (LUAD) is the most common type of non-small cell lung cancer and has the highest mortality rate of all cancers.[1] According to statistics, about 1.6 million people die of lung cancer every year worldwide, of which LUAD accounts for more than 40%.[2] Although treatments for LUAD are being gradually updated, the prognosis for patients with LUAD is still unsatisfactory, with a 5-year survival rate of $< 20\%$.[3] At present, the clinical treatment of LUAD is mainly based on surgical resection of the lesion, and patients with poor prognosis are supplemented by radiotherapy, chemotherapy, and targeted therapy drugs epidermal growth factor receptor (EGFR)-(TKI and ALK-TKI).[4] However, clinical response is usually short-lived, and most cancer patients develop resistance to targeted drugs within a few months,[5] and these drugs often have more severe side effects. Traditional Chinese medicine is a cultural treasure developed in China for thousands of years, not only has low toxicity, and small side effects, but also multi-ingredient, multi-target characteristics are also advantages in treating diseases.[6]

The tuberous root of *Pinellia ternata* (Thunb.) 10. ex Breitenb is the traditional Chinese herb Rhizoma Pinelliae. Rhizoma Coptidis is the dried rhizome of *Coptis Chinensis* Franch. They are a group of herbal combinations commonly found in traditional Chinese medicine compounds.[7] In recent years, the antitumor biological activity of Rhizoma Pinelliae and Rhizoma Coptidis has been confirmed.[8,9] Modern research has found that the mechanism of action of Rhizoma Pinelliae inducing apoptosis of tumor cells is mainly achieved by activating the mononuclear phagocyte system, increasing the level of antioxidant enzymes, and scavenging excessive free radicals.[10] Rhizoma Coptidis exerts antitumor effects by inhibiting tumor extracellular matrix degradation, regulating the cell cycle, and

TM and JL contributed equally to this work.

This article is supported by the National Natural Science Foundation of China (82060784).

The authors have no conflicts of interest to disclose.

All data generated or analyzed during this study are included in this published article [and its supplementary information files].

The present study is a Bioinformatics-based analysis, so ethical and consent permission is unnecessary.

[a] *Graduate School, Heilongjiang University of Chinese Medicine, Harbin, Heilongjiang, China,* [b] *Department of Pharmacy, Baotou Medical College, Baotou, Inner Mongolia, China,* [c] *The First Affiliated Hospital of Heilongjiang University of Chinese Medicine, Harbin, Heilongjiang, China.*

** Correspondence: Hong Chang, Department of Pharmacy, Baotou Medical College, Baotou, Inner Mongolia, China (e-mail: changhong_cool@163.com).*

How to cite this article: Meng T, Liu J, Chang H, Qie R. Reverse predictive analysis of Rhizoma Pinelliae and Rhizoma Coptidis on differential miRNA target genes in lung adenocarcinoma. Medicine 2023;102:7(e32999).

Received: 9 November 2022 / Received in final form: 18 January 2023 / Accepted: 27 January 2023

http://dx.doi.org/10.1097/MD.0000000000032999

inhibiting angiogenesis.[11–13] However, the molecular mechanism of the combination of Rhizoma Pinelliae and Rhizoma Coptidis in the treatment of LUAD has not been clarified. In this study, the material basis and mechanism of Rhizoma Pinelliae and Rhizoma Coptidis in the treatment of LUAD were explored by bioinformatics. In addition, the differential micro-RNA (miRNAs) of Rhizoma Pinelliae and Rhizoma Coptidis in the treatment of LUAD were screened by network analysis.

2. Materials and methods

2.1. Screening and target prediction of active ingredients of "Rhizoma Pinelliae-Rhizoma Coptidis" herb pair

In this study, the HERB database (http://herb.ac.cn/) searched for the compound composition of Rhizoma Pinelliae and Rhizoma Coptidis. The HERB database integrates multiple traditional Chinese medicine databases (Sym Map, TCMID, TCMSP, and TCMD), and high-throughput experiments (microarray and RNA-seq experiments) were performed on the collected data to determine the active ingredients in traditional Chinese medicine. Therefore, the database contains the most comprehensive list of traditional Chinese medicines and ingredients so far.[14] The compounds of Rhizoma Pinelliae and Rhizoma Coptidis are screened by the Swiss ADME platform (http://www.swissadme.ch/).[15] Screening criteria include: Following Lipinski rules, that is, "molecular weight < 500," "Rotatable bonds ≤ 10," "H-bond acceptors ≤ 10," "H-bond donors ≤ 5," and "lipid-water partition coefficient (Log Po/w) ≤ 5"; In pharmacokinetics, GI absorption is "High" and the blood-brain barrier (BBB permeant) is "Yes"; Drug likeness satisfies 3 or more "Yes." Through the Swiss Target Prediction platform, the potential targets of drug compounds are predicted, and targets with "Probability" greater than "0" are screened as potential targets of drugs.

2.2. Screening of differential miRNAs and acquisition of related targets for LUAD

Using "Lung adenocarcinoma" as the keyword, the GEO database (https://www.ncbi.nlm.nih.gov/geo/)[16] retrieved microarray datasets for studies related to LUAD. Through comparison and screening, the chips GSE135918 and GSE128311 were finally included in the study. Two sample sets were analyzed by GEO2R software, and miRNAs were screened with $P < .05$ and $|\log2FC| \geq 1$. The 2 sets of differentially expressed miRNAs were imported into the FunRich3.1.3 software to take the intersection, and the intersecting miRNAs were analyzed by the TargetScanHuman platform (https://www.targetscan.org/vert_72/),[17] and finally, the relevant target genes of LUAD were obtained.

2.3. Target screening and network construction of "Rhizoma Pinelliae-Rhizoma Coptidis" herb pair in the treatment of LUAD

The targets of "Rhizoma Pinelliae-Rhizoma Coptidis" herb pair were combined and intersected with the targets of LUAD. Protein-protein interaction (PPI) of intersecting partial targets is constructed through the String database (https://string-db.org/).[18] The threshold above "0.900" was used as the screening criterion, and the target of "Rhizoma Pinelliae-Rhizoma Coptidis" herb pair for the treatment of LUAD was finally screened. Through Cytoscape 3.8.0 software,[19] the network diagram of "traditional Chinese medicine - active ingredient - therapeutic target - miRNA - disease" was constructed. The top 10 compounds with degree values were screened as core compounds, and it was believed that these compounds played an important role in the treatment of LUAD by "Rhizoma Pinelliae-Rhizoma Coptidis" herb pair.

2.4. Core target screening

The PPI is imported into the Cytoscape software, and the MCODE algorithm is applied to screen out the highly relevant modules and construct a visual network diagram. The algorithm starts the search by weighting the nodes in the network, then selecting the node with high weight as the initial node, and finally filtering out the core targets in the dense area of the original PPI network. The MCODE algorithm parameters are set as follows "degree = 2," "node score cutoff = 0.2," "k-core = 2, max." "Depth = 100."[20] The target protein corresponding to the screening module is considered to be the core target of Rhizoma Pinelliae and Rhizoma Coptidis in the treatment of LUAD.

2.5. Gene ontology (GO) enrichment analysis and Kyoto encyclopedia of genes and genomes (KEGG) pathway enrichment analysis

The core target was imported into the DAVID database, the attribute was set to "Homo sapiens," GO enrichment analysis was performed with $P < .05$ as the condition, and the analysis results of biological processes, molecular functions, and cellular components were displayed through bubble charts. The BioMart platform (http://asia.ensembl.org/biomart/martview/c8e74f900745aa80be4b62038e25607a)[21] was used to convert the gene ID of the core target to Ensemblegene ID. Through Omicshare platform (http://www.omicshare.com/tools/index.php/) conducts KEGG pathway enrichment analysis on core targets. In the KEGG enrichment analysis results, the entries with $P < .001$ were screened, and the top 20 items were plotted as a circle chart. The suitable pathway was screened out in the enrichment pathway, and the enriched target in the pathway was considered to be the key target.

2.6. Molecular docking verification

Download the mol2 format of the 3D structure of core compounds in Banxia and Coptis via the Pubchem database (https://pubchem.ncbi.nlm.nih.gov/).[22] Protein structures of key targets are screened in the PDB database (https://www.rcsb.org/)[23] under the condition that resolution is less than 2.5 and small molecule compounds are attached. Use the DockThor platform (https://dockthor.lncc.br/v2/)[24] to build a suitable docking box and perform molecular docking. Use PyMol 2.4.0 software to visualize the top results.

3. Results

3.1. Acquisition of active ingredients and targets of herbs

A total of 180 active ingredients in Rhizoma Pinelliae and 77 active ingredients in Rhizoma Coptidis were retrieved through the HERB database. After screening, 32 active ingredients of Rhizoma Pinelliae were obtained (Table 1). There are 27 active ingredients in Rhizoma Coptidis were obtained (Table 2). A total of 5715 targets were predicted using the SwissTargetPrediction platform, and a total of 510 targets were obtained by removing "Probability" to "0" and removing duplicate values.

3.2. Differential miRNA expression profile selection and related gene acquisition

The dataset GSE135918 (https://www.ncbi.nlm.nih.gov/geo/query/acc.cgi?acc=GSE135918) has a total of 10 samples, including 2 samples from the LUAD group and 2 samples from the control group. GPL19730 in the dataset GSE128311 (https://www.ncbi.nlm.nih.gov/geo/query/acc.cgi?acc=GSE128311) is an expression profile analysis of miRNA arrays, with a total of 77 samples, including 35 samples in the LUAD group, and 32

Table 1

Active ingredients of Pinellia.

Component	Formula	Molecular weight	Rotatable bonds	H-Bond acceptors	H-Bond donors	Consensus log P	Gi absorption	Bbb permeant	Lipinski	Ghose	Veber	Egan	Muegge
(-)-Citronellal	$C_{10}H_{18}O$	154.3	5	1	0	2.94	High	Yes	Yes	No	Yes	Yes	No
2-Undecanone	$C_{11}H_{22}O$	170.3	8	1	0	3.48	High	Yes	Yes	Yes	Yes	Yes	No
3-Phenylpropionic acid	$C_9H_{10}O_2$	150.2	3	2	1	1.78	High	Yes	Yes	No	Yes	Yes	No
4-Methoxycyclohexanoic acid	$C_8H_8O_3$	152.2	2	3	1	1.49	High	Yes	Yes	No	Yes	Yes	No
6-Shogaol	$C_{17}H_{24}O_3$	276.4	9	3	1	3.76	High	Yes	Yes	Yes	Yes	Yes	Yes
9-Oxononanoic acid	$C_9H_{16}O_3$	172.2	8	3	1	1.71	High	Yes	Yes	Yes	Yes	Yes	No
Anethole	$C_{10}H_{12}O$	148.2	2	1	0	2.79	High	Yes	Yes	No	Yes	Yes	No
Benzaldehyde	C_7H_6O	106.1	1	1	0	1.57	High	Yes	Yes	No	Yes	Yes	No
Bis (4-hydroxybenzyl) ether	$C_{14}H_{14}O_3$	230.3	4	3	2	2.34	High	Yes	Yes	Yes	Yes	Yes	Yes
Butyl vinyl ether	$C_6H_{12}O$	100.2	4	1	0	1.82	High	Yes	Yes	No	Yes	Yes	No
Catechol	$C_6H_6O_2$	110.1	0	2	2	0.97	High	Yes	Yes	No	Yes	Yes	No
Cavidine	$C_{21}H_{23}NO_4$	353.4	2	5	0	3.2	High	Yes	Yes	Yes	Yes	Yes	Yes
Cedrol	$C_{15}H_{26}O$	222.4	0	1	1	3.55	High	Yes	Yes	Yes	Yes	Yes	No
Citral	$C_{10}H_{16}O$	152.2	4	1	0	2.71	High	Yes	Yes	No	Yes	Yes	No
Coniine	$C_8H_{17}N$	127.2	2	1	1	1.99	High	Yes	Yes	No	Yes	Yes	No
Conimine	$C_{22}H_{36}N_2$	328.5	1	2	2	3.84	High	Yes	No	Yes	Yes	Yes	Yes
Crysophanol	$C_{15}H_{10}O_4$	254.2	0	4	2	2.38	High	Yes	Yes	Yes	Yes	Yes	Yes
Ephedrine	$C_{10}H_{15}NO$	165.2	3	2	2	1.46	High	Yes	Yes	Yes	Yes	Yes	No
Ferulic acid	$C_{10}H_{10}O_4$	194.2	3	4	2	1.36	High	Yes	Yes	Yes	Yes	Yes	No
Furfural	$C_5H_4O_2$	96.08	1	2	0	0.69	High	Yes	Yes	No	Yes	Yes	No
Hydroquinone	$C_6H_6O_2$	110.1	0	2	2	0.87	High	Yes	Yes	No	Yes	Yes	No
Methyl 2-chloropropenoate	$C_4H_5ClO_2$	120.5	2	2	0	1.17	High	Yes	Yes	No	Yes	Yes	No
Methylpyrazine	$C_5H_6N_2$	94.11	0	2	0	0.62	High	Yes	Yes	No	Yes	Yes	No
N-(5-methylisoxazol-3-Yl) acetamide	$C_6H_8N_2O_2$	140.1	2	3	1	0.61	High	Yes	Yes	No	Yes	Yes	No
Nonanal	$C_9H_{18}O$	142.2	7	1	0	2.78	High	Yes	Yes	No	Yes	Yes	No
Norharman	$C_{11}H_8N_2$	168.2	0	1	1	2.41	High	Yes	Yes	Yes	Yes	Yes	No
O-methyl ferulic acid	$C_{11}H_{12}O_4$	208.2	4	4	1	1.83	High	Yes	Yes	Yes	Yes	Yes	Yes
P-coumaric acid	$C_9H_8O_3$	164.2	2	3	2	1.26	High	Yes	Yes	Yes	Yes	Yes	No
Protocatechuic aldehyde	$C_7H_6O_3$	138.1	1	3	2	0.8	High	Yes	Yes	No	Yes	Yes	No
Scopoletin	$C_{10}H_8O_4$	192.2	1	4	1	1.52	High	Yes	Yes	Yes	Yes	Yes	No
Spantol	$C_{10}H_{13}NO_2$	179.2	5	2	1	1.8	High	Yes	Yes	Yes	Yes	Yes	No
Valeraldoxime	$C_5H_{11}NO$	101.2	3	2	1	1.32	High	Yes	Yes	No	Yes	Yes	No

samples in the control group. Both datasets were analyzed by miRNA microarrays to obtain differential miRNA expression profiles. Using $P < .05$ and $|\log2FC| \geq 1$ as screening criteria, a total of 652 miRNAs were obtained in the dataset GSE135918. A total of 93 miRNAs were obtained in the dataset GSE128311. Differential miRNA expression is represented as a volcano plot (Fig. 1A and B). The 2 datasets were intersected to obtain 25 differential miRNAs (Fig. 1C). Through the analysis and screening of the target scan human platform, 60,326 related genes were obtained, and 15,323 related genes were obtained after removing duplicates.

3.3. Therapeutic target screening and related network construction

A total of 417 targets were obtained by intersecting the targets of the "Rhizoma Pinelliae-Rhizoma Coptidis" herb pair and LUAD targets (Fig. 2A). Through the String database, protein interaction analysis was conducted on intersection targets, and 1050 interactions were obtained, including 294 protein nodes, namely therapeutic targets. The "Traditional Chinese Medicine-Active Ingredient-Therapeutic-Therapeutic Target-miRNA-Disease" network (Fig. 2B) was constructed using Cytoscape software and network topology analysis was performed, and core compounds were screened out based on the top 10 degree values (Table 3). The most important modules and core targets were screened out by the analysis of protein interactions of therapeutic targets by MCODE plug-ins (Fig. 2C).

3.4. Enrichment analysis results

A total of 1124 GO enrichment analysis results were obtained with $P < .05$ as the screening condition. There are 109 biological processes, including bidirectional regulation of RNA polymerase II promoter transcription, cell signaling, and cell differentiation regulation (Fig. 3A). There are 56 molecular functions, including RNA polymerase II transcription factor activity, ligand activation sequence-specific DNA binding, ion, transcription factor, and protease binding (Fig. 3B); There are 21 cell compositions, including peroxisome matrix, RNA polymerase II transcription factor complex, and polymer complexes (Fig. 3C).

A total of 69 KEGG enrichment analysis results were screened with $P < .001$, and the results showed that cancer-related pathways were the most involved, accounting for 27%, of which the most relevant cancer pathway was non-small cell lung cancer. In addition, the signaling pathway of "Rhizoma Pinelliae-Rhizoma Coptidis" herb pair for the treatment of LUAD is also enriched in immune-related pathways, such as C-type lectin receptor signaling pathway and T cell receptor signaling pathway; Endocrine-related pathways, such as thyroid hormone signaling pathway and estrogen signaling pathway; Cell cycle signaling pathways, such as the forkhead box O signaling pathway; Cell metabolic regulatory pathways, such as the cyclic adenosine monophosphate signaling pathway; Tumor vascular endothelial generating pathways, such as VEGF signaling pathways. These signaling pathways may be the main pathway for the treatment of LUAD with "Rhizoma Pinelliae-Rhizoma Coptidis" herb pair (Fig. 3D).

Table 2

Active ingredients of Coptis.

Component	Formula	Molecular weight	Rotatable bonds	H-Bond acceptors	H-Bond donors	Consensus log P	GI absorption	BBB permeant	Lipinski	Ghose	Veber	Egan	Muegge
(R)-Canadine	$C_{20}H_{21}NO_4$	339.4	2	5	0	2.97	High	Yes	Yes	Yes	Yes	Yes	Yes
2,4-Heptadienal	$C_7H_{10}O$	110.2	3	1	0	1.67	High	Yes	Yes	No	Yes	Yes	No
2,4-Octadienal	$C_8H_{12}O$	124.2	4	1	0	2.07	High	Yes	Yes	No	Yes	Yes	No
2-Octenal	$C_8H_{14}O$	126.2	5	1	0	2.27	High	Yes	Yes	No	Yes	Yes	No
5,8-Dihydroxy-2-(2-phenylethyl) chromone	$C_{17}H_{14}O_4$	282.3	3	4	2	2.91	High	Yes	Yes	Yes	Yes	Yes	Yes
Berberine	$C_{20}H_{18}NO_4$	336.4	2	4	0	2.53	High	Yes	Yes	Yes	Yes	Yes	Yes
Berlambine	$C_{20}H_{17}NO_5$	351.4	2	5	0	3.04	High	Yes	Yes	Yes	Yes	Yes	Yes
Citral	$C_{10}H_{16}O$	152.2	4	1	0	2.71	High	Yes	Yes	No	Yes	Yes	No
Columbamine	$C_{20}H_{20}NO_4$	338.4	3	4	1	2.33	High	Yes	Yes	Yes	Yes	Yes	Yes
Coptisine	$C_{19}H_{14}NO_4$	320.3	0	4	0	2.4	High	Yes	Yes	Yes	Yes	Yes	Yes
Corydaldine	$C_{11}H_{13}NO_3$	207.2	2	3	1	1.34	High	Yes	Yes	Yes	Yes	Yes	Yes
Epiberberine	$C_{20}H_{18}NO_4$	336.4	2	4	0	2.5	High	Yes	Yes	Yes	Yes	Yes	Yes
Ethyl Caffeate	$C_{11}H_{12}O_4$	208.2	4	4	2	1.82	High	Yes	Yes	Yes	Yes	Yes	Yes
Fagarine	$C_{13}H_{11}NO_3$	229.2	2	4	0	2.59	High	Yes	Yes	Yes	Yes	Yes	Yes
Ferulic acid	$C_{10}H_{10}O_4$	194.2	3	4	2	1.36	High	Yes	Yes	Yes	Yes	Yes	No
Groenlandicine	$C_{19}H_{16}NO_4$	322.3	1	4	1	2.18	High	Yes	Yes	Yes	Yes	Yes	Yes
Isovanillin	$C_8H_8O_3$	152.2	2	3	1	1.12	High	Yes	Yes	No	Yes	Yes	No
Jatrorrhizine	$C_{20}H_{20}NO_4$	338.4	3	4	1	2.31	High	Yes	Yes	Yes	Yes	Yes	Yes
Magnoflorine	$C_{20}H_{24}NO_4$	342.4	2	4	2	0.65	High	Yes	Yes	Yes	Yes	Yes	Yes
Magnograndiolide	$C_{15}H_{22}O_4$	266.3	0	4	2	1.7	High	Yes	Yes	Yes	Yes	Yes	Yes
Matsutake alcohol	$C_8H_{16}O$	128.2	5	1	1	2.21	High	Yes	Yes	No	Yes	Yes	No
O-Methylferulic acid	$C_{11}H_{12}O_4$	208.2	4	4	1	1.83	High	Yes	Yes	Yes	Yes	Yes	Yes
Palmatine	$C_{21}H_{22}NO_4$	352.4	4	4	0	2.64	High	Yes	Yes	Yes	Yes	Yes	Yes
P-Coumaric acid	$C_9H_8O_3$	164.2	2	3	2	1.26	High	Yes	Yes	Yes	Yes	Yes	No
Phellodendrine	$C_{20}H_{24}NO_4$	342.4	2	4	2	0.45	High	Yes	Yes	Yes	Yes	Yes	Yes
Worenine	$C_{20}H_{16}NO_4$	334.4	0	4	0	2.69	High	Yes	Yes	Yes	Yes	Yes	Yes
Zosimin	$C_{19}H_{20}O_5$	328.4	4	5	0	3.4	High	Yes	Yes	Yes	Yes	Yes	Yes

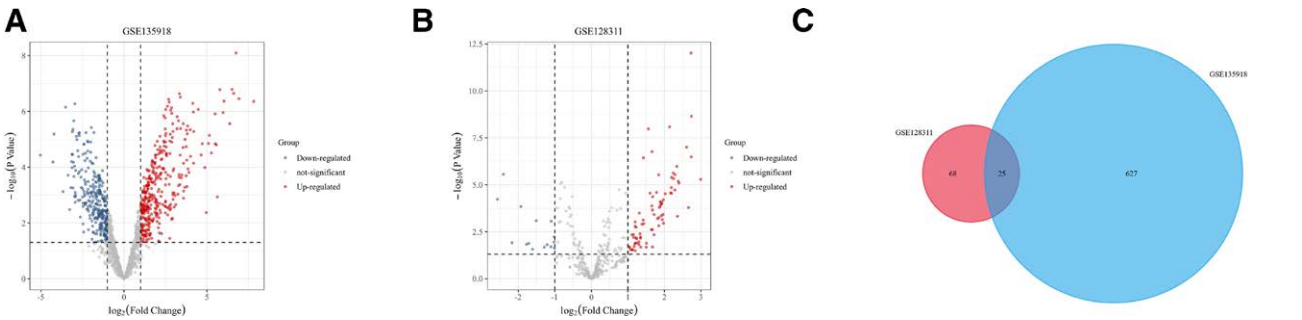

Figure 1. The differential miRNA volcano map of the dataset GSE135918, with a total of 380 up-regulated miRNAs and 272 down-regulated miRNAs (A). The differential miRNA volcano map of the dataset GSE128311, with a total of 78 miRNAs up-regulated and 15 miRNAs down-regulated (B). The Venn plot of the intersection of differential miRNAs in 2 datasets (C). miRNA = micro RNA.

3.5. Molecular docking results

In the KEGG results, the non-small cell lung cancer pathway was the most significant, so the 10 targets enriched on this pathway (EGFR, Janus Kinase 3, mitogen-activated protein kinase 1, phosphatidylinositol-4, 5-bisphosphate 3-kinase catalytic subunit alpha, phosphoinositide-3-kinase regulatory subunit 1, protein kinase C alpha, retinoic acid receptor beta, retinoid x receptor alpha, retinoid x receptor gamma, signal transducer and activator of transcription 3) were used as key targets for molecular docking with core compounds. According to the heat map of docking results (Fig. 4A), all docking scores were < -5.0 kcal/mol, the average docking score was −7.55 kcal/mol, and the docking score of ≤ -7.0 kcal/mol accounted for 73.0%, so the core compounds in the "Rhizoma Pinelliae-Rhizoma Coptidis" herb pair had the good binding ability to key targets. Among them, the compounds with better binding ability were Palmatine, Berberine, and Berlambine. Visualize the result with the highest score of the 3 combinations through PyMol (Fig. 4B–D).

4. Discussion

As one of the deadliest malignant tumors in the world, LUAD has always attracted the attention of scholars from all over the world. When most patients are diagnosed, they are already in the advanced stage of LUAD, because of its insidious onset and small lesions. At present, modern medicine has limited means of treating LUAD, and many patients turn their attention to the medicine of the motherland. As a cultural treasure of the Chinese nation, Chinese medicine has a significant effect on the treatment of intractable diseases, and its natural advantages of multiple ingredients have gradually been recognized by many scholars.[2,5] In this study, the commonly used anti-tumor Chinese herbal medicine combination: "Rhizoma Pinelliae-Rhizoma Coptidis" herb pair, analyzed the mechanism of action of the 2 in the treatment of LUAD by integrating network technology, and obtained the difference miRNA and target genes between "Rhizoma Pinelliae-Rhizoma Coptidis" herb pair in the treatment of LUAD by reverse matching, and verified the results through molecular docking.

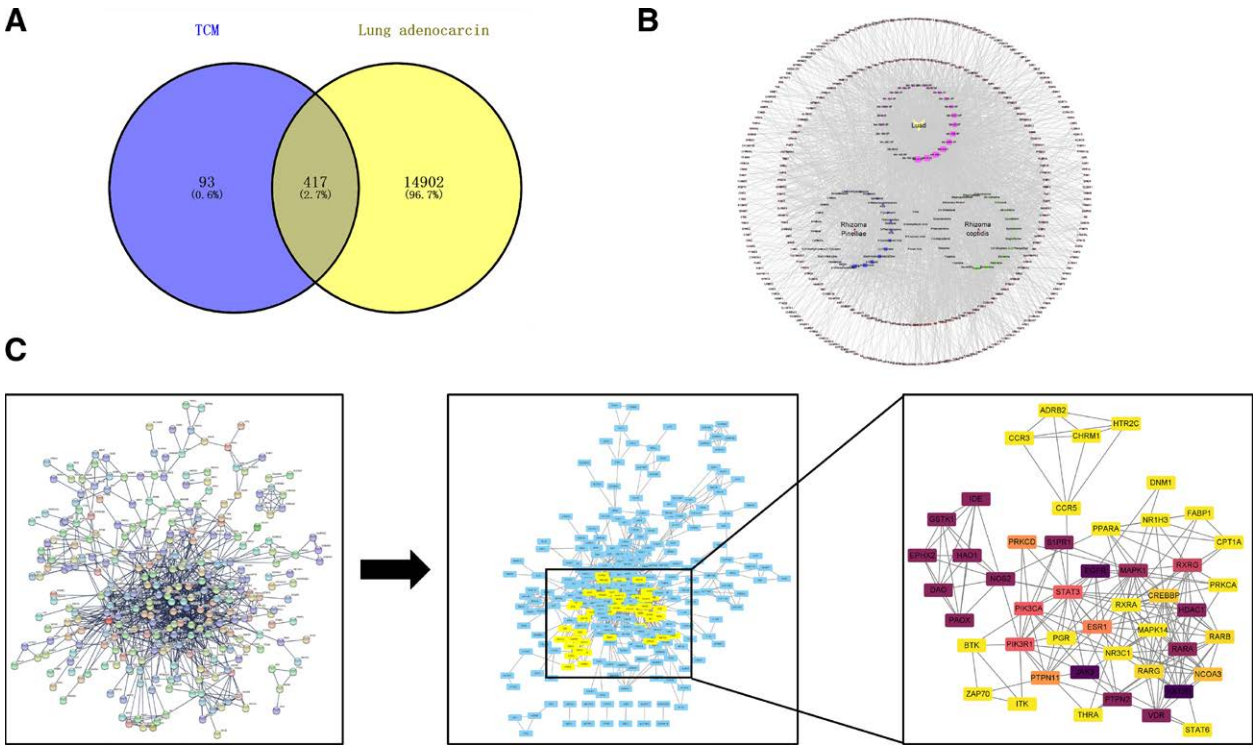

Figure 2. The Venn diagram of the herb and disease intersection target (A). The network diagram of "Traditional Chinese Medicine-Active Ingredient-Therapeutic Target-miRNA-Disease" (B). The module analysis and core target screening network diagram, the darker the color, the higher the importance of the target in the network (C). miRNA = micro RNA.

Table 3

Topological analysis of core compounds.

Name	Degree	Average shortest path length	Betweenness centrality	Closeness centrality
Cavidine	74	2.413793103	0.017390208	0.414285714
2-Undecanone	70	2.440318302	0.017644867	0.409782609
Zosimin	64	2.461538462	0.012928191	0.40625
Berlambine	61	2.4933687	0.010971259	0.40106383
6-Shogaol	58	2.514588859	0.011055308	0.397679325
Bis (4-hydroxybenzyl) ether	54	2.535809019	0.010722681	0.394351464
(-)-Citronellal	51	2.546419098	0.009951934	0.392708333
Palmatine	46	2.557029178	0.00573066	0.391078838
Berberine	44	2.583554377	0.004843539	0.387063655
9-Oxononanoic acid	43	2.631299735	0.005664846	0.380040323

The unbalanced expression of miRNAs is a key factor to promote the rapid occurrence and development of tumors, and the expression profiles of miRNAs are generally characterized in tumor tissues, and the expression profiles of these tumor cells are significantly different from the normal cell expression profiles in the same tissue, so the expression of miRNAs is more accurate to distinguish the type of tumor than the mRNA encoded by proteins.[26] The difference between Rhizoma Pinelliae and Rhizoma Coptidis in the treatment of LUAD in this study found a total of 25 miRNAs, and through searching domestic and foreign literature, it was found that these miRNAs were all related to cancer, of which 10 (miR-126-5P,[27] miR-22-5P,[28] miR-183-5P,[29] miR-144-3P,[30] miR-340-5P,[31] miR-142-5P,[3] miR-200A-3P,[32] miR-429,[33] miR-200B-3P,[34] miR-3648[35]) are directly associated with LUAD. At the same time, the pathway with the highest significance of "Rhizoma Pinelliae-Rhizoma Coptidis" herb pair in the treatment of LUAD found in this study is the non-small cell lung cancer pathway, and the key target with the highest degree of freedom value is EGFR. At present, EGFR is considered to be the most common driver gene for LUAD,[36] which coincides with the results of this study. Therefore, miRNAs with a strong correlation with EGFR in this study are expected to become potential biomarkers affecting the development of LUAD, and in addition to miRNAs that have been reported to be directly related to LUAD, 4 miRNAs that are expected to be biomarkers for the identification of the occurrence and progression of LUAD are screened in this study.

miR-5703 is a driver of cell proliferation, miR-5703 promotes adenocarcinoma cell proliferation by binding to CKLF Like MARVEL transmembrane domain containing 4 and downregulates its expression.[37] Inhibition of miR-5703 has a down-regulating effect on adenocarcinoma-derived exosomes, which directly inhibits the proliferation of adenocarcinoma cells.[38] Similarly, overexpression of miR-3125 reduces levels of the pyruvate dehydrogenase kinase 1 protein in cells, increasing the chance of adenocarcinoma.[39] miR-652-5P has been demonstrated in several studies for its potential as a tumor marker.[40] Interestingly, the expression of miR-652-5P in plasma samples

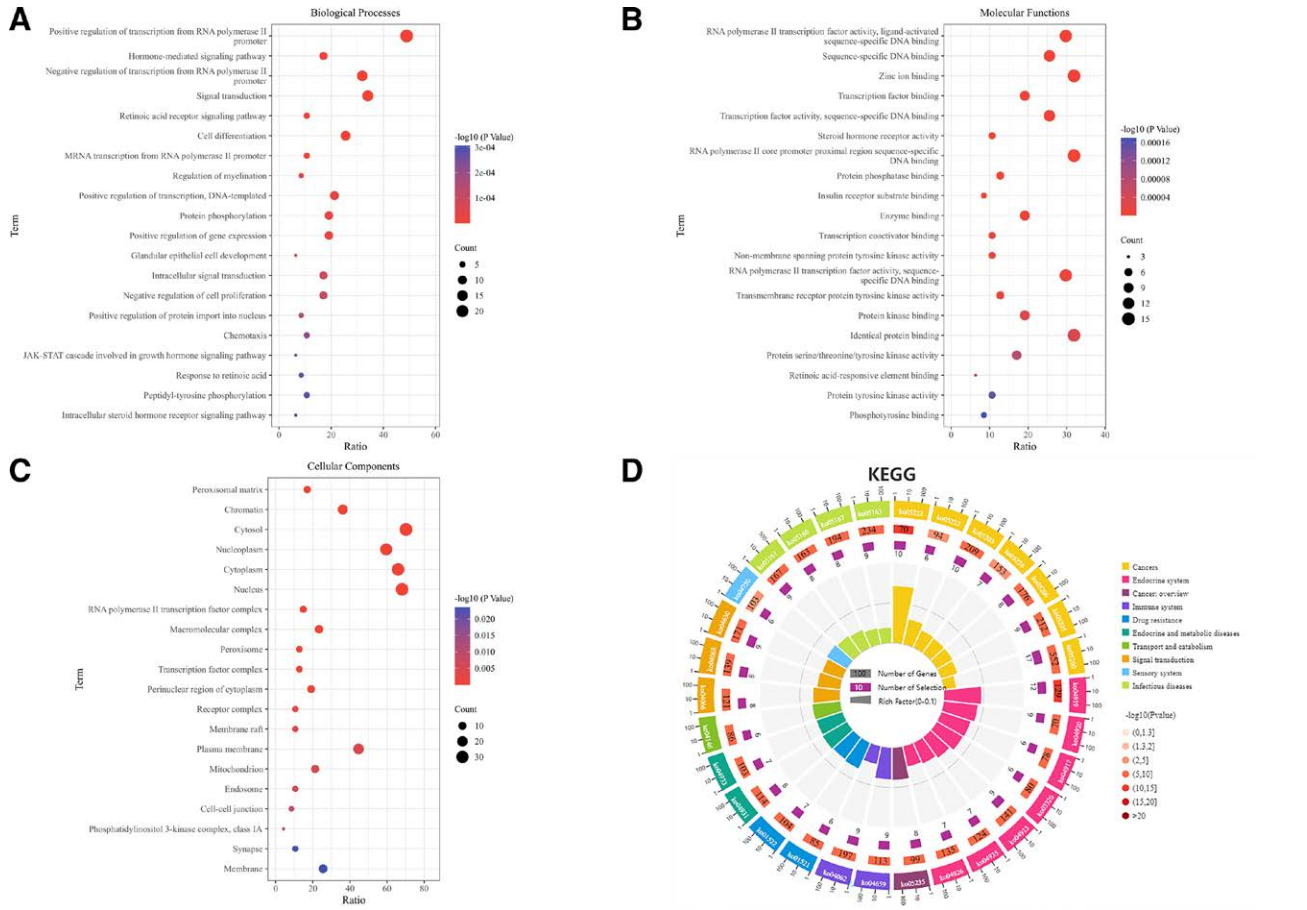

Figure 3. The bubble plot of biological process results in GO enrichment analysis (A). The bubble plot of molecular function results in GO enrichment analysis (B). The bubble plot of cell composition results in GO enrichment analysis. The color from red to blue in the bubble chart indicates that the "*P*" value is getting higher, and the larger the bubble, the more genes are enriched in entry (C). The top 30 KEGG pathways are significantly the most relevant, with the length of the bar corresponding to the number of background genes, the depth of the color corresponding to the "*P*" value, and the darker the color, the smaller the value (D). GO = gene ontology. KEGG = Kyoto encyclopedia of genes and genomes.

from patients with adenocarcinoma was higher than that of normal people,[41] while the reverse was true for patients with squamous cell carcinoma.[40] miR-513c-5p is a tumor suppressor gene that regulates cell proliferation, migration, and invasion.[42] The study found that miR-513c-5p targets lysophosphatidic acid receptor 5 and inhibits its expression. High expression of lysophosphatidic acid receptor 5 tends to predict higher rates of lymphatic metastasis and distant metastases, as well as lower overall survival of adenocarcinoma.[43] This result may make miR-513c-5p a potential biomarker of the degree of metastasis of cancer cells. All 4 miRNAs affected the proliferation and migration of adenocarcinoma, and they had a strong correlation with EGFR in this study. Therefore, miR-5703, miR-3125, miR-652-5P, and miR-513c-5p are promising potential biomarkers for identifying different stages of LUAD development and determining cancer types.

Molecular docking results showed that the compounds with outstanding binding ability were Palmatine, Berberine, and Berlambine, which all belonged to alkaloids. Alkaloids exert significant antitumor effects mainly by inhibiting tumor cell proliferation, promoting apoptosis and autophagy, and regulating tumor angiogenesis and tumor metastasis.[44] In addition, studies have proved that alkaloid-containing traditional Chinese medicines have good pharmacological effects on targeting the tumor microenvironment.[45] Modern pharmacology shows that Berberine has the characteristics of low toxicity to healthy cells and high toxicity to cancer cells, which makes Berberine one of the most promising natural anticancer drugs.[46] Berberine can effectively inhibit the proliferation and migration of LUAD.[47] The study found that berberine blocked DNA replication in LUAD cells by down-regulating DNA polymerase epsilon 2 and DNA primase subunit 1 in LUAD cells. At the same time, Berberine has a down-regulating effect on the main gene expression biomarker (forkhead box M1) that can reflect the poor prognosis of pan-cancer,[47] which indicates that berberine has a good inhibitory effect on the development of LUAD cells throughout the cycle. Palmatine is a class of isoquinoline alkaloids with highly effective biological activity and good water solubility and has shown a good effect in promoting apoptosis of adenocarcinoma cells in previous studies.[48,49] Studies have shown that palmatine inhibits the activation of collagen type 1 alpha 1 and survivin mediated by glioma-associated oncogene 1, thereby inhibiting adenocarcinoma cell proliferation and promoting apoptosis.[50] At the same time, palmatine can inhibit lung metastasis of adenocarcinoma cells and prevent lung structural changes, which is achieved by upregulating the expression of tumor suppressor p53 and thus inhibiting the transcription of metastasis-associated protein 1.[51]

5. Conclusion and outlook

In this study, the differential miRNAs of LUAD were mined by bioinformatics technology, and the targets and related pathways enriched by "Rhizoma Pinelliae-Rhizoma Coptidis" herb pair were screened out by network analysis, and the differential miRNA in the treatment of LUAD were reverse-matched

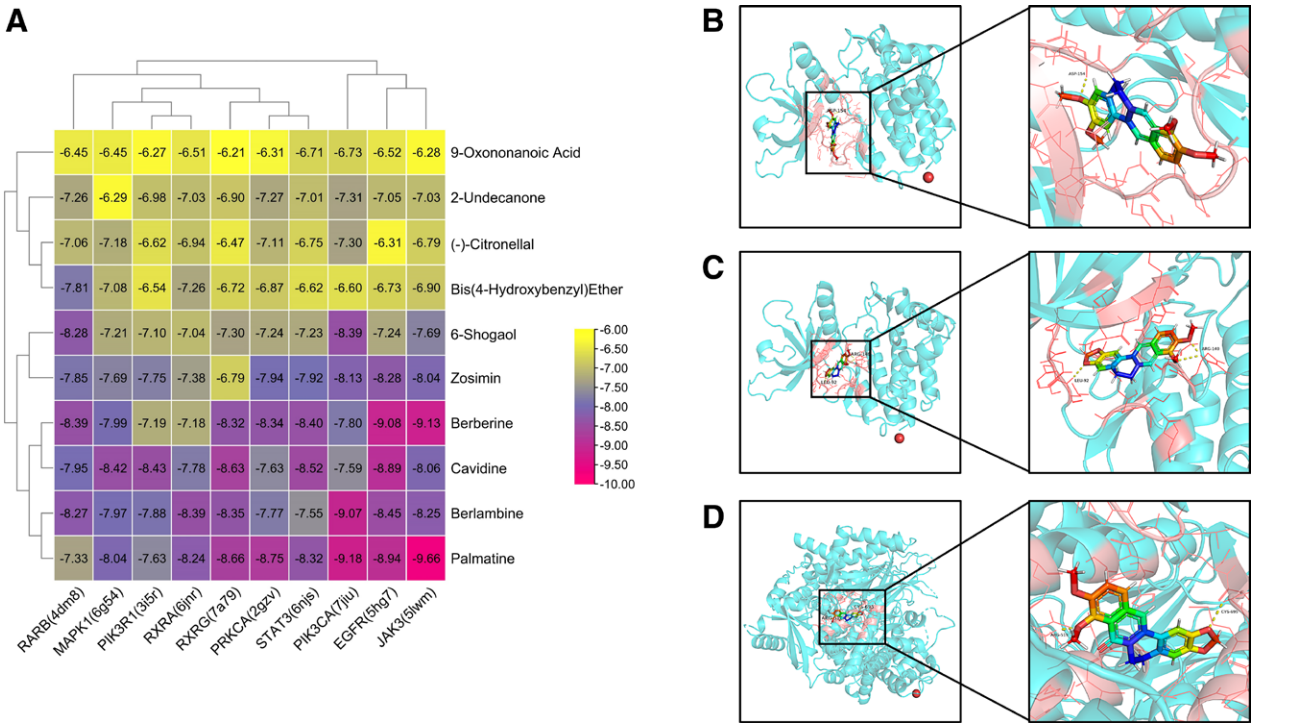

Figure 4. The heat map of molecular docking results, the color is from yellow to purple, and the docking score is gradually reduced (A). The schematic diagram of the binding of the compound Palmatine to the target JAK3, and aspartic acid forms a hydrogen bond at position 154 (B). The schematic diagram of the binding of the compound Berberine to the target JAK3, forming 2 hydrogen bonds at position 140 arginine and 1 hydrogen bond at position 92 isoleucine (C). The schematic diagram of the combination of compound Berlambine and target PIK3CA forms one hydrogen bond at position 519 arginine and cysteine at position 695, respectively (D). JAK3 = Janus Kinase 3. PIK3CA = phosphatidylinositol-4,5-bisphosphate 3-kinase catalytic subunit alpha.

by the herb. It is ultimately believed that miR-5703, miR-3125, miR-652-5P, and miR-513c-5p may become new biomarkers for the treatment of LUAD. Through the analysis of molecular docking results, alkaloids may be the main components of "Rhizoma Pinelliae-Rhizoma Coptidis" herb pair for the treatment of LUAD, mainly by inhibiting tumor cell proliferation, promoting apoptosis, and regulating tumor metastasis.

In summary, this study explores the targets, herb components, differential miRNAs, and pathways of "Rhizoma Pinelliae-Rhizoma Coptidis" herb pair in the treatment of LUAD, which provides a key reference basis and data support for elucidating the mechanism of action of traditional Chinese medicine in the treatment of LUAD and assisting in prevention in the future, and also lays a preliminary foundation and provides direction for follow-up research. In addition, the differential miRNAs and core targets screened by bioinformatics in this study need to be verified by subsequent experiments to ensure the accuracy and reliability of the results.

Author contributions

Funding acquisition: Hong Chang.
Supervision: Rui Qie.
Visualization: Tianwei Meng.
Writing – original draft: Jiawen Liu.
Writing – review & editing: Rui Qie.

References

[1] Li H, Tong L, Tao H, et al. Genome-wide analysis of the hypoxia-related DNA methylation-driven genes in lung adenocarcinoma progression. Biosci Rep. 2020;40.
[2] Dong Q, Yu P, Ye L, et al. PCC0208027, a novel tyrosine kinase inhibitor, inhibits tumor growth of NSCLC by targeting EGFR and HER2 aberrations. Sci Rep. 2019;9:5692.
[3] Jia Y, Duan Y, Liu T, et al. LncRNA TTN-AS1 promotes migration, invasion, and epithelial mesenchymal transition of lung adenocarcinoma via sponging miR-142-5p to regulate CDK5. Cell Death Dis. 2019;10:573.
[4] Ren KH, Qin WW, Wang Y, et al. Detection of an EML4-ALK fusion mutation secondary to epidermal growth factor receptor-tyrosine kinase inhibitor (EGFR-TKI) therapy for lung cancer: a case report. Ann Palliat Med. 2022;11:2503–9.
[5] Denisenko TV, Budkevich IN, Zhivotovsky B. Cell death-based treatment of lung adenocarcinoma. Cell Death Dis. 2018;9:117.
[6] Wang Y, Yang S, Zhang S, et al. Oxymatrine inhibits proliferation and migration of vulvar squamous cell carcinoma cells via attenuation of the RAS/RAF/MEK/ERK pathway. Cancer Manag Res. 2020;12:2057–67.
[7] Liang G, Zhang L, Jiang G, et al. Effects and components of herb pair huanglian-banxia on diabetic gastroparesis by network pharmacology. Biomed Res Int. 2021;2021:8257937.
[8] Huang H, Zhang M, Yao S, et al. Immune modulation of a lipid-soluble extract of Pinellia pedatisecta Schott in the tumor microenvironment of an HPV (+) tumor-burdened mouse model. J Ethnopharmacol. 2018;225:103–15.
[9] Cao Q, Hong S, Li Y, et al. Coptisine suppresses tumor growth and progression by down-regulating MFG-E8 in colorectal cancer. RSC Adv. 2018;8:30937–45.
[10] Hu M, Liu Y, Wang L, et al. Purification, characterization of two polysaccharides from Pinelliae Rhizoma praeparatum cum alumine and their anti-inflammatory effects on mucus secretion of airway epithelium. Int J Mol Sci. 2019;20:3553.
[11] Chen DX, Pan Y, Wang Y, et al. The chromosome-level reference genome of coptis chinensis provides insights into genomic evolution and berberine biosynthesis. Hortic Res. 2021;8:121.
[12] Kim SH, Kim EC, Kim WJ, et al. Coptis japonica Makino extract suppresses angiogenesis through regulation of cell cycle-related proteins. Biosci Biotechnol Biochem. 2016;80:1095–106.
[13] Wang N, Tan HY, Li L, et al. Berberine and Coptidis Rhizoma as potential anticancer agents: recent updates and future perspectives. J Ethnopharmacol. 2015;176:35–48.
[14] Fang S, Dong L, Liu L, et al. HERB: a high-throughput experiment- and reference-guided database of traditional Chinese medicine. Nucleic Acids Res. 2021;49:D1197–206.

[15] Daina A, Michielin O, Zoete V. Swiss ADME: a free web tool to evaluate pharmacokinetics, drug-likeness and medicinal chemistry friendliness of small molecules. Sci Rep. 2017;7:42717.
[16] Edgar R, Domrachev M, Lash AE. Gene expression omnibus: NCBI gene expression and hybridization array data repository. Nucleic Acids Res. 2002;30:207–10.
[17] Friedman RC, Farh KK, Burge CB, et al. Most mammalian mRNAs are conserved targets of microRNAs. Genome Res. 2009;19:92–105.
[18] Szklarczyk D, Franceschini A, Kuhn M, et al. The STRING database in 2011: functional interaction networks of proteins, globally integrated and scored. Nucleic Acids Res. 2011;39:D561–8.
[19] Shannon P, Markiel A, Ozier O, et al. Cytoscape: a software environment for integrated models of biomolecular interaction networks. Genome Res. 2003;13:2498–504.
[20] Tian Y, Xing Y, Zhang Z, et al. Bioinformatics analysis of key genes and circRNA-miRNA-mRNA regulatory network in gastric cancer. Biomed Res Int. 2020;2020:2862701.
[21] Smedley D, Haider S, Ballester B, et al. BioMart--biological queries made easy. BMC Genomics. 2009;10:22.
[22] Kim S, Thiessen PA, Bolton EE, et al. PubChem substance and compound databases. Nucleic Acids Res. 2016;44:D1202–13.
[23] Berman H, Henrick K, Nakamura H, et al. The worldwide Protein Data Bank (wwPDB): ensuring a single, uniform archive of PDB data. Nucleic Acids Res. 2007;35:D301–3.
[24] Santos KB, Guedes IA, Karl ALM, et al. Highly flexible ligand docking: benchmarking of the dockthor program on the LEADS-PEP protein-peptide data set. J Chem Inf Model. 2020;60:667–83.
[25] Zhu XY, Guo DW, Lao QC, et al. Sensitization and synergistic anti-cancer effects of furanodiene identified in zebrafish models. Sci Rep. 2019;9:4541.
[26] Jang JY, Kim YS, Kang KN, et al. Multiple microRNAs as biomarkers for early breast cancer diagnosis. Mol Clin Oncol. 2021;14:31.
[27] Liu B, Wang R, Liu H. mir-126-5p promotes cisplatin sensitivity of non-small-cell lung cancer by inhibiting ADAM9. Biomed Res Int. 2021;2021:6622342.
[28] Wu C, Bian X, Zhang L, et al. Long noncoding RNA LINC00968 inhibits proliferation, migration and invasion of lung adenocarcinoma through targeting miR-22-5p/CDC14A axis. 3 Biotech. 2021;11:433.
[29] He RQ, Gao L, Ma J, et al. Oncogenic role of miR-183-5p in lung adenocarcinoma: a comprehensive study of qPCR, in vitro experiments and bioinformatic analysis. Oncol Rep. 2018;40:83–100.
[30] Liu C, Yang Z, Deng Z, et al. Downregulated miR-144-3p contributes to progression of lung adenocarcinoma through elevating the expression of EZH2. Cancer Med. 2018;7:5554–66.
[31] Liu D, Lin L, Wang Y, et al. PNO1, which is negatively regulated by miR-340-5p, promotes lung adenocarcinoma progression through Notch signaling pathway. Oncogenesis. 2020;9:58.
[32] Gong D, Zhao ZW, Zhang Q, et al. The long noncoding RNA metastasis-associated lung adenocarcinoma transcript-1 regulates CCDC80 expression by targeting miR-141-3p/miR-200a-3p in vascular smooth muscle cells. J Cardiovasc Pharmacol. 2020;75:336–43.
[33] Cao L, Zhou X, Ding X, et al. Knockdown of circ-PVT1 inhibits the progression of lung adenocarcinoma and enhances the sensitivity to cisplatin via the miR-429/FOXK1 signaling axis. Mol Med Rep. 2021;24.
[34] Liu K, Zhang W, Tan J, et al. MiR-200b-3p functions as an oncogene by targeting ABCA1 in lung adenocarcinoma. Technol Cancer Res Treat. 2019;18:1533033819892590.
[35] Tu Y, Mei F. miR-3648 promotes lung adenocarcinoma-genesis by inhibiting SOCS2 (suppressor of cytokine signaling 2). Bioengineered. 2022;13:3044–56.
[36] Masago K, Kuroda H, Takahashi Y, et al. Synchronous driver gene alterations (EGFR L858R, T790M, and ROS1) rearrangements in a patient with early-stage lung adenocarcinoma. Cancer Gen. 2022;268-269:124–7.
[37] Li M, Guo H, Wang Q, et al. Pancreatic stellate cells derived exosomal miR-5703 promotes pancreatic cancer by downregulating CMTM4 and activating PI3K/Akt pathway. Cancer Lett. 2020;490:20–30.
[38] Pranavkrishna S, Sanjeev G, Akshaya RL, et al. A computational approach on studying the regulation of TGF-β1-stimulated runx2 expression by microRNAs in human breast cancer cells. Comput Biol Med. 2021;137:104823.
[39] Subramaniam S, Jeet V, Gunter JH, et al. Allele-specific microRNA-mediated regulation of a glycolysis gatekeeper PDK1 in cancer metabolism. Cancers (Basel). 2021;13:3582.
[40] Gao P, Wang D, Liu M, et al. DNA methylation-mediated repression of exosomal miR-652-5p expression promotes ossophageal squamous cell carcinoma aggressiveness by targeting PARG and VEGF pathways. PLoS Genet. 2020;16:e1008592.
[41] Lagendijk M, Sadaatmand S, Koppert LB, et al. MicroRNA expression in pre-treatment plasma of patients with benign breast diseases and breast cancer. Oncotarget. 2018;9:24335–46.
[42] Xia HL, Lv Y, Xu CW, et al. MiR-513c suppresses neuroblastoma cell migration, invasion, and proliferation through direct targeting glutaminase (GLS). Cancer Biomark. 2017;20:589–96.
[43] Tong C, Wang C, Wang Y, et al. TNRC6C-AS1 promotes thyroid cancer progression by upregulating LPAR5 via miR-513c-5p. Cancer Manag Res. 2021;13:6141–55.
[44] Liu C, Yang S, Wang K, et al. Alkaloids from traditional Chinese medicine against hepatocellular carcinoma. Biomed Pharmacother. 2019;120:109543.
[45] Casey SC, Vaccari M, Al-Mulla F, et al. The effect of environmental chemicals on the tumor microenvironment. Carcinogenesis. 2015;36(Suppl 1):S160–83.
[46] Kim JS, Oh D, Yim MJ, et al. Berberine induces FasL-related apoptosis through p38 activation in KB human oral cancer cells. Oncol Rep. 2015;33:1775–82.
[47] Ni L, Sun P, Fan X, et al. Berberine inhibits FOXM1 dependent transcriptional regulation of POLE2 and interferes with the survival of lung adenocarcinoma. Front Pharmacol. 2021;12:775514.
[48] Wu J, Xiao Q, Zhang N, et al. Palmatine hydrochloride mediated photodynamic inactivation of breast cancer MCF-7 cells: effectiveness and mechanism of action. Photodiagn Photodyn Ther. 2016;15:133–8.
[49] Wu J, Xiao Q, Zhang N, et al. Photodynamic action of palmatine hydrochloride on colon adenocarcinoma HT-29 cells. Photodiagn Photodyn Ther. 2016;15:53–8.
[50] Chakravarthy D, Muñoz AR, Su A, et al. Palmatine suppresses glutamine-mediated interaction between pancreatic cancer and stellate cells through simultaneous inhibition of survivin and COL1A1. Cancer Lett. 2018;419:103–15.
[51] Ativui S, Danquah CA, Ossei PPS, et al. Palmatine attenuates metastatic lung colonization of triple negative breast cancer cells. Front Pharmacol. 2022;13:853230.